01 Jan 1993

Robust Control Of Flexible Structures Using Multiple Shape Memory Alloy Actuators

R. Lashlee

R. Butler

Vittal S. Rao
Missouri University of Science and Technology

F. Kern

Recommended Citation

R. Lashlee et al., "Robust Control Of Flexible Structures Using Multiple Shape Memory Alloy Actuators," *1st IEEE Regional Conference on Aerospace Control Systems, AEROCS 1993 - Proceedings*, pp. 798 - 804, article no. 721043, Institute of Electrical and Electronics Engineers, Jan 1993.
The definitive version is available at https://doi.org/10.1109/AEROCS.1993.721043

Robust Control of Flexible Structures Using Multiple Shape Memory Alloy Actuators

Robert Lashlee, Robert Butler,
Vittal Rao, and Frank Kern
Department of Electrical Engineering and Intelligent Systems Center
University of Missouri-Rolla, Rolla, Mo. 65401

Abstract

The design and implementation of control strategies for large, flexible smart structures presents challenging problems. To demonstrate the capabilities of shape-memory-alloy actuators, we have designed and fabricated a three-mass test article with multiple shape-memory-alloy (NiTiNOL) actuators. The force and moment actuators were implemented on the structure to examine the effects of control structure interaction and to increase actuation force. These SMA actuators exhibit nonlinear effects due to deadband and saturation. The first step in the modeling process was the experimental determination of the transfer function matrix derived from frequency response data. A minimal state space representation was determined based on this transfer function matrix. Finally in order to reduce the order of the controller, a reduced order state space model was derived from the minimal state space representation. The simplified analytical models are compared with models developed by structural identification techniques based on vibration test data.

From the reduced order model, a controller was designed to dampen vibrations in the test bed. To minimize the effects of uncertainties on the closed-loop system performance of smart structures, a LQG/LTR control methodology has been utilized. An initial standard LQG/LTR controller was designed; however, this controller could not achieve the desired performance robustness due to saturation effects. Therefore, a modified LQG/LTR design methodology was implemented to accommodate for the limited control force provided by the actuators. The closed-loop system response of the multiple input-multiple output (MIMO) test article with robustness verification has been experimentally obtained and presented in the paper. The modified LQG/LTR controller demonstrated performance and stability robustness to both sensor noise and parameter variations.

1.0 Introduction

In recent years there has been considerable interest in the design and implementation of active controllers for smart structures. The application of both piezo-electric and shape memory alloy materials as actuators and sensors in the active control of structures has been extensively reported in the literature. We have utilized the shape memory alloy (SMA), NiTiNOL, in the design and implementation of multivariable robust controllers. In addition to the design of multivariable robust controllers, this research examines the effects of control-structure interaction using SMA actuators on a flexible structures. To implement and evaluate the performance of various controllers, we have designed and fabricated a three-mass test article equipped with strain gauge sensors, force and moment SMA actuators, and signal processing circuits. The force and moment SMA actuators allow the application of increased control force and the investigation of control-structure interaction.

In order to design active controllers for flexible structures, a mathematical representation of the system is needed. This system contains inherent nonlinearities resulting from both deadband and saturation characteristics of the SMA actuators; however, a linear model will be used for controller development. First, a transfer function matrix was obtained using experimental frequency response data. Next, a minimal state space realization was generated from the transfer function matrix. Finally, a balancing and truncation method was used to acquire a reduced order model. To minimize the effects of parameter variations, model inaccuracies, and disturbances on the closed-loop system performance of the structure, a LQG/LTR controller was implemented; although, this structure could not meet the desired robustness characteristics without saturating the SMA actuators. Therefore, a modified LQG/LTR methodology was utilized to accommodate the limited control force provided by the SMA actuators. Experimental results demonstrated that the modified controller showed improved robustness characteristics in comparison with the standard LQG/LTR design without saturating the SMA actuators.

This paper is organized as follows. A description of the test article and associated hardware is presented in Section 2. Section 3 contains the modeling methods. The robust control design and implementation methodologies have been presented in Section 4. Finally, The closed-loop performance results are given in Section 5.

2.0 Test Article and Equipment

A test structure was designed for use as a MIMO system. It consists of three steel masses suspended vertically by thin aluminum struts. The masses were chosen such that the structure would have multiple natural frequencies within the limited bandwidth of the NiTiNOL wire actuators. This test article is depicted in Figure (1).

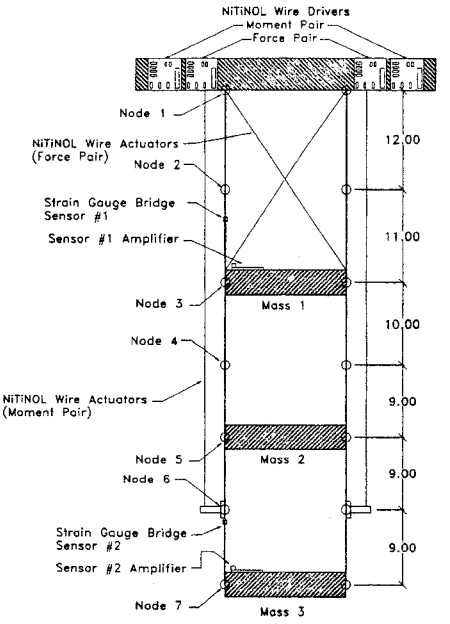

Figure 1. Test Article

Actuation of the structure is accomplished with two sets of NiTiNOL wires with drivers to provide heating. One set of wires, arranged vertically along each strut, applies a moment at the bottom of the structure. A second set of wires, connected diagonally from the top of one strut to a point on the opposite strut just above the top mass, exerts a force on the structure. The NiTiNOL wire used is uncoated, pre-trained, nine mil wire with a transition temperature of 35°C. Each wire is clamped to the beam with an initial tension of 0.5 lbs. The tension in each wire is measured with a load cell mounted in line with the wire. The wires are driven such that the current supplied for one wire is 180° out of phase with the current of the other driver in the pair. Each driver circuit has adjustments for gain, bias and dead-band. A small dead band is allowed in the driver circuit so that current is never applied simultaneously to both wires.

A second component of the dead band is the SMA actuator itself. Since the actuation force is a function of the temperature of the SMA wire, small amounts of current flow through the wire with no resulting force. The relation between the DC voltage applied to the driver and the resulting force in one of the moment actuators is shown in Figure (2). From this figure, it can be seen that the deadband of the SMA actuator for the DC input is approximately 1.6 volts. The actual deadband during operation of the system will vary from the DC value due to the heating and cooling of the NiTiNOL actuator. The dead-band has the benefit of increasing the noise immunity of the actuator.

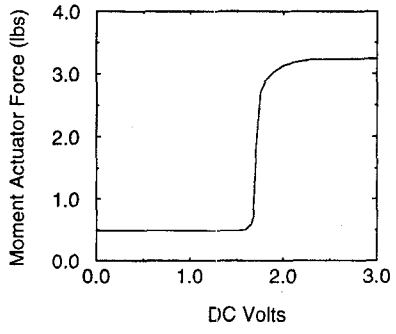

Figure 2. NiTiNOL Force Characteristics

The test structure can be excited with a wide range of initial conditions. Large amplitude initial conditions can permanently deform the NiTiNOL wire force actuators. This is seen as a loss of pretension of the actuator after the controller has quelled vibration in the beam and it is once again at rest. This deformation of the SMA actuators results in system parameter variations. The experimental data presented in this paper is the response with the beam excited in the first mode and the bottom mass displaced by one inch. This moderate amplitude initial condition was chosen to limit the permanent deformation of the force SMA actuators.

Two sets of full bridge strain gauges are bonded to the struts at the locations indicated in Figure (1). The signal conditioning electronics for each bridge are mounted on a mass and are located as close to the bridge as possible to minimize measurement noise. The signal conditioning electronics consist of the necessary balancing resistors for the strain gauge bridge and a fixed gain instrumentation amplifier. The entire bridge plus electronics package is calibrated in volts per microstrain.

For purposes of implementing the digital controllers, the strain gauge electronic circuits are interfaced to a personal computer through a Keithley-Metrabyte DAS-20 A/D board with a SSH-4 simultaneous sample and hold interface. This allows the strain gauge data collection for control as well as the collection of other data of interest such as wire load cell information. The driver circuits are interfaced to the personal computer through a Keithley-Metrabyte DDA-06 simultaneous output D/A board. This arrangement allows implementation of controls over a wide range of sampling frequencies with no sampling skew on either input or output. A block diagram of the experimental setup is shown in Figure (3).

3.0 System Modeling

3.1 Development of the Transfer Function Matrix (TFM)

An experimental model was obtained for the test article from frequency response data acquired with a HP35665A dynamic signal analyzer. Four transfer functions were obtained for the two input-two output system. For each measurement, the analyzer's source sweeps the desired frequencies in a series of very small steps. The input signal power is automatically adjusted at each frequency in the sweep to provide the optimal signal to noise ratio. An advantage of this swept sine measurement is that all of the energy in the frequency response test is concentrated at the desired frequency which gives good excitation of the structural system [1]-[3]. Modal frequencies taken from the bode plots of the system are listed in Table (1). From this table it can be seen that the frequency of the modes is a function of the actuator used to excite the beam. The frequency of the modes is also dependent upon the initial tension in the SMA wires.

TABLE 1.

Mode	Experimental - Force Actuators (Hz)	Experimental - Moment Actuators (Hz)
1	0.96	0.90
2	2.54	2.37
3	3.31	3.09

For each of the four transfer functions, a model was generated by the HP analyzer's built-in curve fitting program. The curve fitting program derives a linear system model from the measured frequency response data. A pole/zero model is developed by calculating a weighted least squares fit of the frequency response data to a rational polynomial. The curve fitting is performed in the s-domain so that the program determines the transfer function. Due to control-structure interaction, each actuator generates two 8th order transfer functions with similar complex poles. A common denominator for all 4 transfer functions was then generated by compromising between the two sets of frequencies [4]. The measured transfer functions and the resulting "fitted" curves are shown in Figure (4).

The corresponding numerators were modified so that the four transfer functions could be written as shown below:

$$\begin{bmatrix} Y_1(s) \\ Y_2(s) \end{bmatrix} = H(s) \begin{bmatrix} U_1(s) \\ U_2(s) \end{bmatrix} \quad \text{where} \quad H(s) = \frac{1}{d(s)} \begin{bmatrix} N_{11} & N_{12} \\ N_{21} & N_{22} \end{bmatrix} \tag{1}$$

$$d(s) = s^8 + 2.89s^7 + 6.82 \times 10^2 s^6 + 1.77 \times 10^3 s^5 + 1.21 \times 10^5 s^4 + 10^5 s^4 + 2.75 \times 10^5 s^3 + 3.64 \times 10^6 s^2 + 7.42 \times 10^6 s + 3.95 \times 10^6$$

$$N_{11} = 8.48 \times 10^{-1} S^5 + 2.53 s^4 + 3.07 \times 10^2 s^3 + 1.17 \times 10^3 s^2 + 1.32 \times 10^4 s + 7.68 \times 10$$

$$N_{12} = -3.14 \times 10^{-1} s^3 - 1.64 \times 10^3 s^2 - 2.42 \times 10^3 s - 1.10 \times 10^3$$

$$N_{21} = 2.18 \times 10^{-3} s^6 + 4.59 \times 10^{-1} s^5 + 2.06 s^4 - 1.11 \times 10^2 s^3 - 3.24 \times 10^2 s^2 - 3.19 \times 10^2 s - 1.04 \times 10^2$$

$$N_{22} = -1.96 S^5 \times -9.85 \times s^4 - 5.31 \times 10^2 s^3 - 1.36 \times 10^3 s^2 - 1.12 \times 10^3 (s) - 2.81 \times 10^3$$

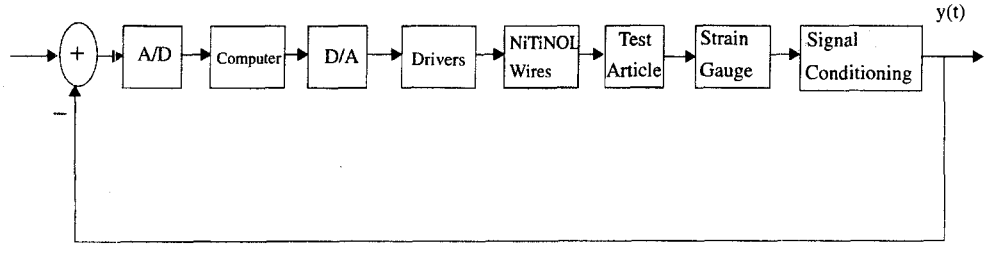

Figure 3. Experimental Block Diagram

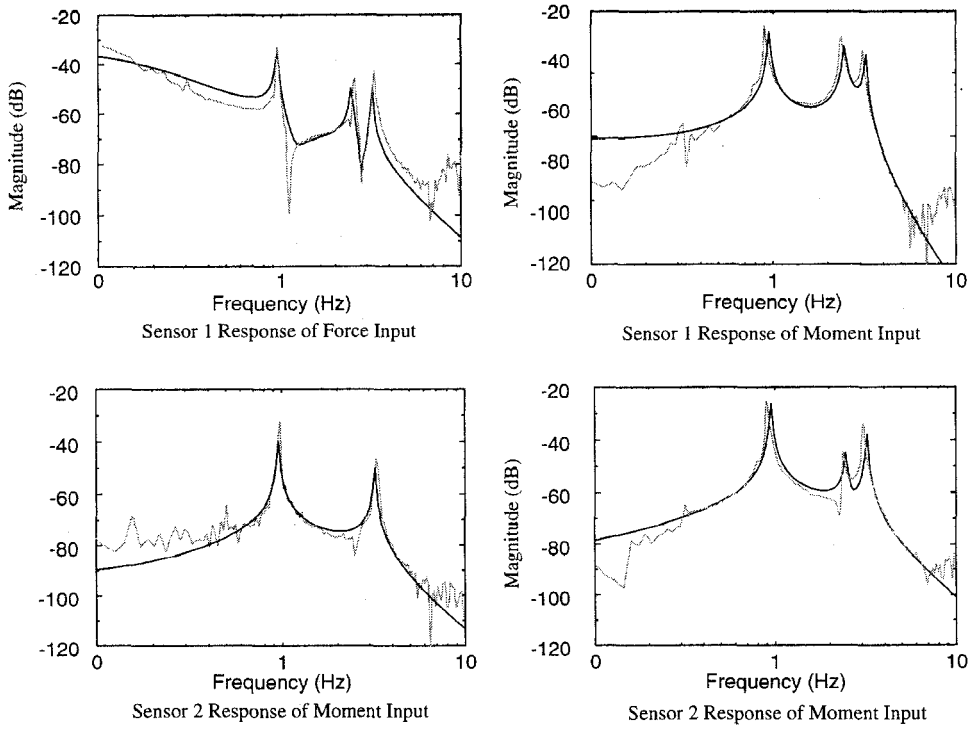

Figure 4. Measured Transfer Functions (Dashed) and Fitted Curves (Solid)

3.2 Determination of State Variable Representation from TFM

Even thought the transfer function matrix has been determined, the a state space representation is needed for the model so that LQG/LTR controllers can be designed. The desired form of the model is contained below:

$$\dot{\underline{x}} = A_p\underline{\hat{x}} + B_p\underline{u}$$
$$\underline{\hat{y}} = C_p\underline{\hat{x}} + D_p\underline{u} \tag{2}$$

The state space realization will be a controller-form realization from a right matrix fraction description (MFD) [5],[6]. First, the TFM must be in the form of a strictly proper right MFD having the form given below:

$$H(s) = N(s)\,D^{-1}(s) \tag{3}$$

In order to obtain a strictly proper right MFD, the TFM was transformed into a Smith McMillian form given below:

$$H(s) = \frac{\Lambda(s)}{d(s)} \tag{4}$$

After performing pole/zero cancellations in the Smith McMillan form, the minimal order of the system was determined to be 14. The minimal order, column reduced transfer function matrix is given below:

$$H(s) = N_r(s)\,D_r^{-1}(s) \tag{5}$$

Once the TFM is in the form of a strictly proper right MFD, a controller form state space realization can be obtained. First, rewrite $D_r(s)$ as

$$D_r(s) = D_{hc}S(s) + D_{lc}\Psi(s) \tag{6}$$

where,

$$S(s) = diag(s^{k_1}, s^{k_2})$$

$$\Psi^T(s) = \begin{bmatrix} s^{k_1-1} & s^{k_1-2} & \dots & s & 1 & 0 \\ 0 & & s^{k_2-1} & s^{k_2-2} & \dots & s & 1 \end{bmatrix}$$

and k_1, k_2 are the column degrees of $D_r(s)$, $D_{hc(s)}$ is the highest column degree coefficient matrix of $D_r(s)$.

Once the matrices in Equation (6) are determined, the state space realization can be formed using the matrix definitions given below [5]:

$$A_p^o = \text{block diag}\left(\begin{bmatrix} 0 & \bigcirc \\ 1 & \ddots \\ & \ddots \\ \bigcirc & 1\ 0 \end{bmatrix},\ k_i x k_i,\ i = 1, 2\right) \tag{7}$$

$$(B_p^o)^T = \text{block diag}([1\ 0 \dots 0],\ 1 \text{ x } k_i,\ i = 1, 2) \tag{8}$$

$$C_p^o = I_2 \tag{9}$$

Finally, the state space matrices are obtained using the following equations.

$$A_p(s) = A_p^o - B_p^o D_{hc}^{-1} D_{lc} \tag{10}$$

$$B_p = B_p^o D_{hc}^{-1} \tag{11}$$

$$C_p = N_{lc} \tag{12}$$

where,

$$N_r = N_{lc}\Psi(s)$$

3.3 Formulation of Reduced Order State Space Model

Next to reduce the order of the controller and allow for the modelling and control of complex systems, a reduced order model was developed. The reduced order model of the system was acquired utilizing the balance and truncation methodology [7]. First, an internally balanced representation of the system is obtained in which the controllability and observability Gramians (Σ) are equal and diagonal.

$$\Sigma = diag(\sigma_1, \sigma_2, \dots, \sigma_n) \tag{13}$$

with

$$\sigma_1 \geq \sigma_2 \geq \dots \geq \sigma_n$$

The σ_i's are Hankel singular values. The order of the reduced order model is determined by retaining the dominant Hankel singular values. Once the dominant values have been determined, the state space model is partitioned as shown below:

$$\begin{bmatrix} A_{bal} & B_{bal} \\ C_{bal} & D_{bal} \end{bmatrix} = \left[\begin{bmatrix} A_{11} & A_{12} \\ A_{21} & A_{22} \end{bmatrix} \begin{bmatrix} B_1 \\ B_2 \end{bmatrix} \right] \\ \left[\begin{bmatrix} C_1 & C_2 \end{bmatrix} \quad D\right] \tag{14}$$

where $A_{11} \in R^{r \times r}$, $A_{22} \in R^{(n-r)\times(n-r)}$, r is the number of dominated Hankel singular values, and $(n-r)$ is the number of nondominate values.

Finally, after the partitioning is completed, the reduced order model is determined by [7]:

$$\begin{aligned} \dot{\hat{x}}_r &= A_r \hat{x}_r + B_r u \\ \hat{y}_r &= C_r \hat{x}_r + D_r u \end{aligned} \tag{15}$$

where,

$$A_r = A_{11}; \qquad B_r = B_1$$
$$C_r = C_1 \qquad D_r = D$$
$$\hat{x}_r = \textit{reduced order state vector}$$

This is the model used for controller development.

3.4 Modelling Results

A comparison of the frequency response of the transfer function matrix and the reduced order model is given in Figure 5. This figure shows that the reduced order model produces a close representation of the response of the transfer function matrix.

4.0 Controller Design

After we acquired the reduced order model of the system, we designed a controller to quell the vibrations in the test article. Difficulties in the controller design stem from parameter variations, linearized model and sensor noise. To overcome these difficulties, we decided to design a robust controller using LQG/LTR methodology. The block diagram of the controller and plant is shown in Figure (6).

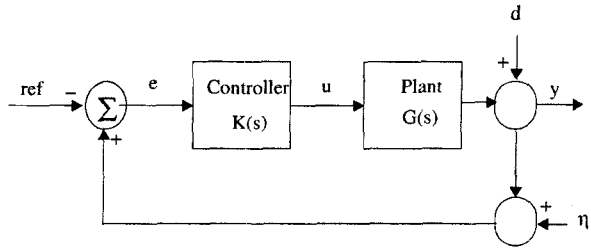

Figure 6. Block Diagram of the Controller and the Plant

The LQG/LTR controller is designed based on Equation (16) and (17). More details on the fundamental equations used for the LQG/LTR controller design are contained in [8]-[11].

$$\dot{x}(t) = A\underline{x}(t) + B\underline{u}(t) + \Gamma \underline{w}(t) \tag{16}$$

$$J = \lim_{T\to\infty} E\{\int_0^T (\underline{x}^T(t)\, Q_c \underline{x}(t) + \underline{u}^T(t)\, R_c \underline{u}(t))\, dt\} \tag{17}$$

Once the filter gains (K_f) and the regulator gains (K_c) are obtained, the controller is then implemented using the state equations in Equation (18).

$$\begin{aligned} \dot{X}_c &= (A - BK_c - K_f C) X_c + K_f e \\ U_c &= -K_c X_c \end{aligned} \tag{18}$$

An initial controller design was performed without restricting the control effort. Even thought we have not obtained accurate loop transfer recovery, we see from Figure (7) that we are already saturating the actuators (control effort > 5.0V). Therefore, we decided to reduce the amount of recovery until we acquired a controller that would no longer saturate the actuators. The maximum control effort produced by this controller was 4.0V; however, the closed loop performance was poor. Therefore, we needed to develop a controller that would be insensitive to system uncertainties without saturating the SMA actuators. We turned to a modified structure for the LQG/LTR controller developed by Prakash [7] which quicken the loop transfer recovery process. This quickening of the loop transfer recovery process can be shown using the error expression, E_o, defined as the error between the desired loop shape and the actual loop

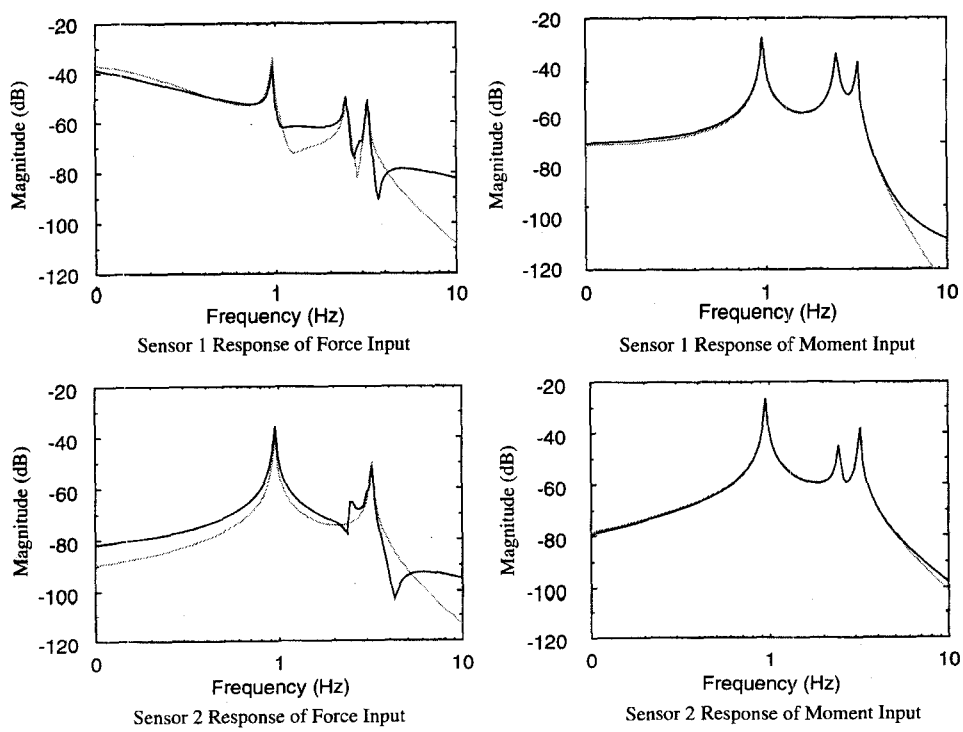

Figure 5. Frequency Response Comparison (solid - reduced order model, dashed - TFM)

shape at the output of the plant. Equation (19) contains E_0 for the nominal LQG/LTR structure.

$$E_o(s) = (I + C_r \Phi K_f)(I + N(s))^{-1} N(s) \tag{19}$$

where

$$N(s) = C_r (sI - A_r + B_r K_c)^{-1} K_f \tag{20}$$

While, Equation (21) contains the expression for the modified structure.

$$E_o(s) = N(s) \tag{21}$$

Note that perfect recovery is obtained when $E_0 = 0$. Now, for all s, as k_c is increased, Equation (21) becomes small more quickly than Equation (19) [7]. This shows that the modified structure produces more accurate loop transfer recovery for a given k_c. This modified structure is shown in Figure (8).

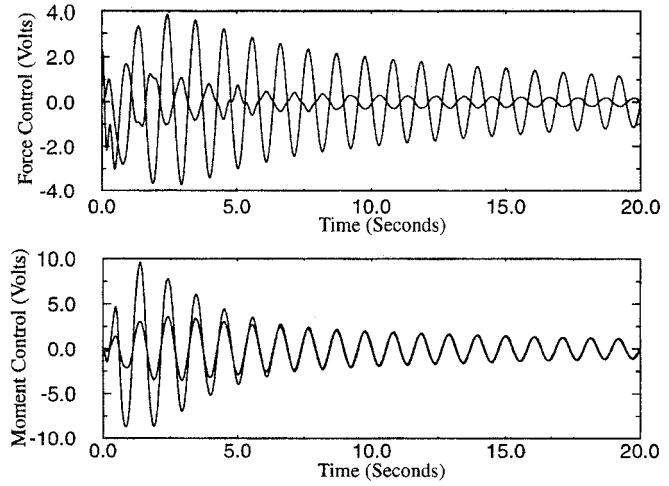

Figure 7. Comparison of Controller Effort

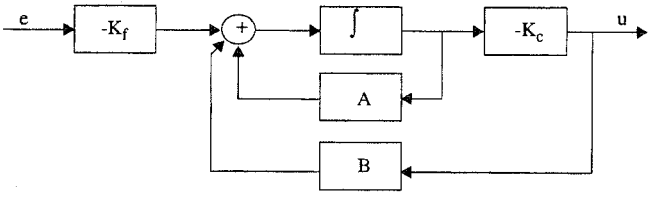

Figure 8. Block Diagram of Modified Structure

Prakash [7] showed that this structure does produce a stable closed-loop system as long as the recovery is exact enough. If the system is unstable k_c must be increased until the recovery is exact enough to produce a stable system. The implementation equation used for this modified structure is given in Equation (22).

$$\begin{aligned} \dot{X}_c &= (A - BK_c) X_c + K_f e \\ U &= -K_c X_c \end{aligned} \tag{22}$$

Using this structure, we designed a new controller. This controller had accurate loop transfer recovery while not saturating the SMA actuators (see Figure (8)).

5.0 Experimental Results

In order to verify the robustness properties of the controllers, operating parameters of the system were varied. The first study involved testing robustness in the presence of sensor noise. The second study consisted of a mass variation to test robustness due to modeling inaccuracies.

Figure (9) shows the open loop response of the test article when excited in the first mode. The open-loop damping will be shown in all of the following closed-loop plots using the open-loop envelopes as shown in this figure. The first mode initial condition responses for the standard LQG/LTR and the modified LQG/LTR controllers are shown in Figure (10). This figure indicates that the modified LQG/LTR controller out performed the standard LQG/LTR controller. The modified LQG/LTR took approximately 2.5 seconds for the control signal to become greater that the deadband and then suppressed the vibrations to the deadband level in approximately 7.5 seconds. The standard LQG/LTR took approximately 2 seconds for the control signal to become greater that the deadband and then suppressed the vibrations to the deadband level in approximately 12 seconds.

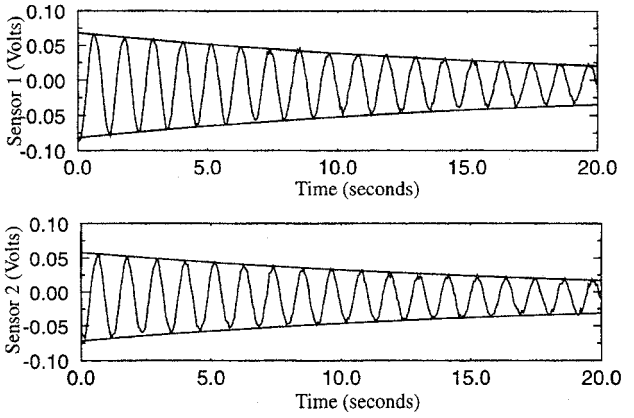

Figure 9. Open-Loop Time Response

In order to test the robustness of the controllers, a parameter variation robustness test was conducted by adding mass to the structure. The second and third masses were increased by 1.4 lbs. Figure (11) contains the experimental system responses. With this parameter variation, both controllers were able to damped the oscillations to the deadband level in approximately 15 seconds. Another robustness test was performed using normally distributed noise signals with a variance of 400 and a mean of zero added to the sensor values to increase the sensor noise. Figure (12) contains the noise corrupted sensor values and the actual system response for both of the controllers. Even though the signal to noise ratio is poor, the modified LQG/LTR controller damped the oscillations to the deadband level in approximately 10 seconds, while the standard LQG/LTR controller was unstable.

6.0 Conclusions

A method to utilize SMA actuators in the control of a MIMO flexible structure is presented in this paper. A flexible structure test article incorporating force and moment SMA actuators, strain gauge sensors, and signal processing electronic circuits was designed and fabricated in our laboratory. First, a transfer function matrix was obtained experimentally using frequency response data. Next, a state space model was formulated from the transfer function matrix. Finally, a reduced order design model was acquired using balancing and truncation methodology. From this reduced order model, a modified LQG/LTR controller was designed and implemented. This controller displayed insensitivity to the inherent SMA actuator nonlinearities. It also successfully exhibited robustness to both sensor noise and parameter variations without saturating the SMA actuators. Future investigation will focus on the development of controllers which specifically address the system nonlinearities such as the deadband and saturation associated with the SMA actuators.

7.0 Acknowledgments

This research is supported by a grant from the U. S. Army research office (Grant number DAAL03-90-G-0053). The support and technical interest of Dr. Gary Anderson, the technical monitor of the project is gratefully acknowledged. Captain Lashlee is grateful to Air Force Academy for sponsoring his graduate studies.

8.0 References

1. Söderström, T., and Stoica, P., System Identification, pp 37-42, Prentice-Hall, Inc. 1987.

2. Ljung, L., System Identification: Theory for the User, pp 143-146, Prentice-Hall, Inc. 1987.

3. Moore, B. C., "On the Flexibility offered by State Feedback in Multivariable Systems beyond Closed-Loop Eigenvalue Assignment", *IEEE Transactions on Automatic Control*, Volume AC-21, pp 689-692, 1976.

4. Grace, A., Lamb, A. J., Little, J.N., Thompson, C., "Control Systems Toolbox for use with MATLAB", The Mathworks, Inc., October 1990.

5. Kailath, Thomas, Linear Systems, Prentice-Hall, Inc. 1980.

6. Chen, Chi-Tsong, Linear System Theory and Design, Holt, Rinehart and Winston. 1984.

7. Prakash, Rajiva, Target Feedback Loop/Loop Transfer Recovery Robust Control System Designs, Dissertation, Department of Electrical Engineering, University of Missouri-Rolla, 1990.

8. Doyle, J.C. and Stein, G., "Multivariable Feedback Design: Concepts for a Classical/Modern Synthesis", *IEEE Transactions on Automatic Control,* Volume. AC-24, Feb 1981, pp 607-611.

9. Maciejowski, J.M., Multivariable feedback design, Addison-Wesley Publishing Co., 1989.

10. Ridgely, D. and Banda, S., "Introduction to Robust Multivariable Control," AFWAL-TR-85-3102, United States Air Force, February 1986.

11. Tebbe, Chris, "Modeling and Robust Control of Smart Structures," *1993 North American Conference on Smart Structures and Materials*, 1993.

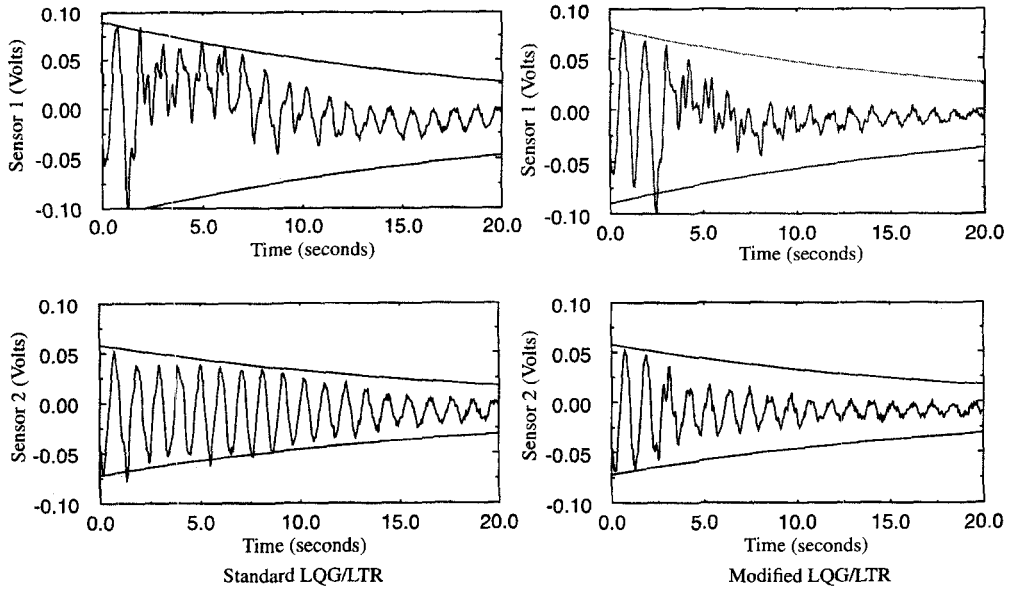

Figure 10. Controller Responses

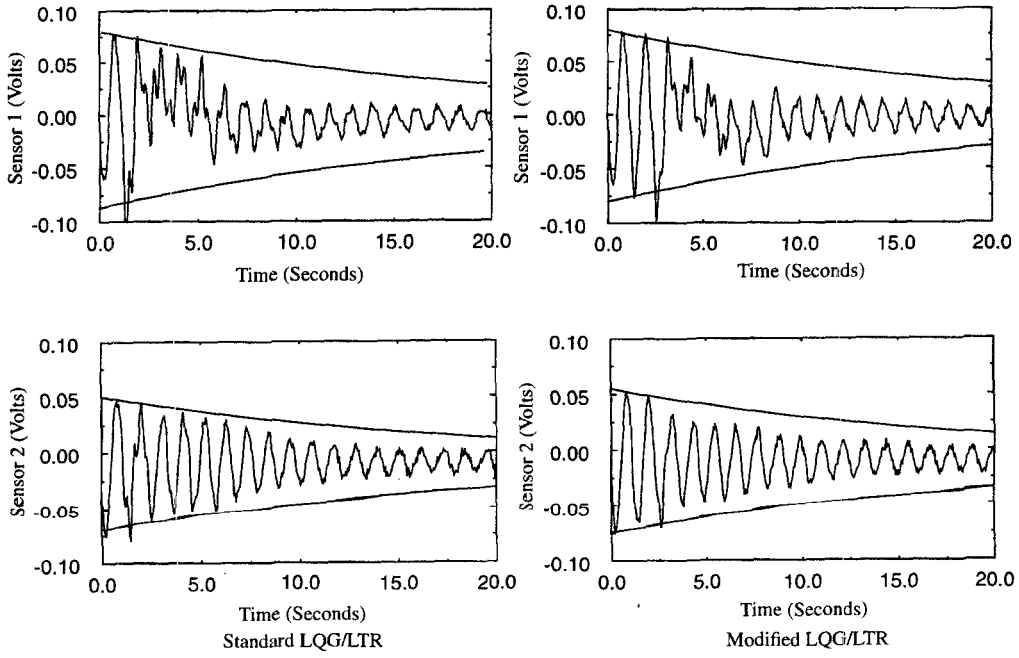

Figure 11. Controller Response With Added Mass

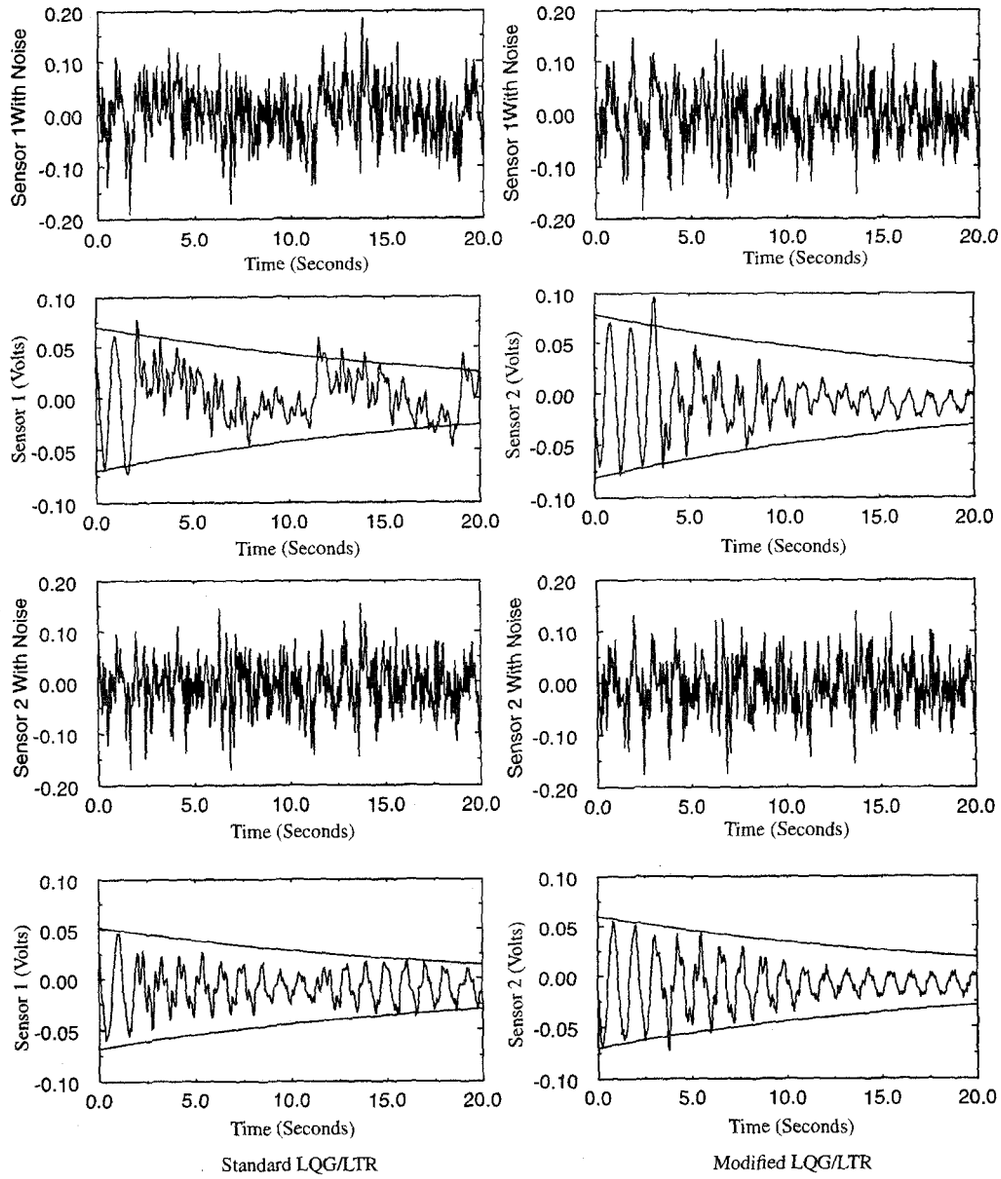

Figure 12. Controller Responses With Added Noise